

Article

Preparation and Acoustic Performance of Porous Aerogel Composites of Graphene Oxide and Cellulose

Jinbao Shao ^{1,2,†}, Yuexiao Lv ^{1,2,†}, Zhenhua Xue ^{1,2,*}, Yanfei Pan ^{1,2,*} , Jinwei Liu ^{1,2}, Mayin Dai ^{1,2} and Fengqi Qiu ^{1,2}

¹ College of Material Science and Art Design, Inner Mongolia Agricultural University, Hohhot 010018, China; s15538970502@163.com (J.S.); lyx19930011@imau.edu.cn (Y.L.); jinwei0505@gmail.com (J.L.); daimayin@emails.imau.edu.cn (M.D.); 15848368579@163.com (F.Q.)

² Inner Mongolia Key Laboratory for Sand Shrubs Fibrosis and Energy Development and Utilization, Hohhot 010018, China

* Correspondence: x_zhenhua@126.com (Z.X.); panyanfeiz@imau.edu.cn (Y.P.)

† These authors contributed equally to this work.

Abstract: In this study, sound insulation materials with a high sound absorption coefficient were prepared. In this paper, using cellulose (CEL) and graphene oxide (GO) as the main raw materials and epichlorohydrin as the cross-linker, the CEL-GO composite aerogels were prepared via lyophilisation. The structure, molecular bonding, and acoustic absorption mechanisms of the composite aerogel were characterised and analysed using SEM, FTIR, XRD, BET, and Raman. In addition, corresponding molecular structure models were constructed. The acoustic attenuation of the CEL-GO composite aerogel was measured using a standing wave tube acoustic attenuation tester. The results show that the chemical bond between the GO and CEL composite is established, and the addition of graphene makes the pores of the composite more advanced, which is more favorable for sound absorption, and the acoustic absorption coefficient can reach up to 0.87.

Keywords: cellulose; graphene oxide; aerogel; microstructure; acoustic absorption coefficient



Citation: Shao, J.; Lv, Y.; Xue, Z.; Pan, Y.; Liu, J.; Dai, M.; Qiu, F. Preparation and Acoustic Performance of Porous Aerogel Composites of Graphene Oxide and Cellulose. *Coatings* **2024**, *14*, 441. <https://doi.org/10.3390/coatings14040441>

Academic Editor: Alina Pruna

Received: 7 March 2024

Revised: 3 April 2024

Accepted: 3 April 2024

Published: 8 April 2024



Copyright: © 2024 by the authors. Licensee MDPI, Basel, Switzerland. This article is an open access article distributed under the terms and conditions of the Creative Commons Attribution (CC BY) license (<https://creativecommons.org/licenses/by/4.0/>).

1. Introduction

Noise has become one of the three major sources of pollution in the world, and it is becoming increasingly severe [1]. Prolonged exposure to noisy environments can make people irritable and cause physiological damage to the human body, such as hearing loss and nerve damage [2]. Noise pollution has received widespread attention from various countries. Existing ways to solve noise pollution mainly start by controlling the propagation mode and source of sound waves. By reasonably designing the structure and arrangement layout of sound-absorbing materials, the propagation path and source of sound waves can be effectively controlled to achieve the purpose of sound absorption and noise reduction [3]. High-porosity structures (>90%) attenuate sound energy by increasing the effective friction between air and pore walls [4] and are currently the mainstay of sound-absorbing materials. Among them, porous bodies produced by petroleum-based polymers and rock- and slag-based fibres are dominant due to their low prices [5–8]. However, these synthetic porous materials rely on non-renewable resources and generate pollutants (such as SO_x and NO_x) during the manufacturing process [9,10], thereby emitting large amounts of greenhouse gases [7,11,12]. The disposal of synthetic sound-absorbing materials, especially polymer foam materials at the end of use, will also cause further environmental problems [8,13]. Therefore, people are gradually shifting their focus toward natural materials. T. Yang et al. [7] summarised the sound absorption performance of natural fibre materials and found that many natural fibres have good sound absorption performance, and some natural fibres are ideal substitutes for glass fibres.

As a traditional acoustic material, wood is a natural, green, and sustainable porous composite material. According to the testing results of the Wood Industry Research Institute of the Chinese Academy of Forestry, the air dry density of most of China's main wood is in the range of 0.2–0.75 g·cm⁻³ [14], and it is estimated that its porosity is between 51% and 87%. But the porosity of individual tree species, such as light wood, reached 94% [15]. There are not only macroscopic pores such as cell cavities in wood, but also nanopores in the cell wall [16], with a porosity of about 7.1% [17]. The relatively low porosity of natural wood makes it highly reflective [18], making it difficult to become an excellent sound-absorbing and noise-reducing material [19–21]. Recently, scientists have developed porous wood-based materials through a top-down process using chemical treatment [22–28] and fungal corrosion [29] methods. Wang [24] prepared porous wood sponges by selectively removing lignin and hemicellulose, followed by freeze-drying; Hu [25] delignified large natural wood and converted it into a porous wood aerogel; Zhao [30] prepared insulating wood with a porosity of up to 93% using a comprehensive process of in situ delignification, solvent exchange, and air drying. The sound absorption coefficient was close to 80% at 2500 Hz. H. Kolya [31] used ammonium persulfate treatment to enhance the sound absorption ability of Malas hardwood, improving breathability and the average sound absorption coefficient in each frequency range of 500–6400 Hz; Zhu Xiaodong [32] summarised the sound absorption performance of wood plastic composite materials. When the perforation rates are 6% and 9%, the sound absorption coefficient increases with the depth of the cavity. The arrangement of carbon atoms in graphene is bonded in sp² hybridisation orbitals, as in graphite monolayers, forming a honeycomb layered structure of hexagonal rings with high strength and toughness. Zhou [33] used magnesium sulfate and tetradecyl betaine as raw materials to prepare a porous acoustic material based on alkali magnesium sulfate (BMS) cement, and the experimental results showed that the acoustic absorption coefficient of the material was 0.70; Li [34] composited low-density aerogel with polyurethane to prepare acoustic materials with a void-like structure, and the experimental results showed that the average acoustic absorption coefficient of the material was 0.71; Pang [35] composited ultra-thin graphene film with polymer foam to prepare a high-frequency acoustic material, making full use of the honeycomb network structure of graphene, and the experimental results showed that the maximum acoustic absorption coefficient could reach 0.8 in the range of 200–6000 Hz; Zong [36] prepared acoustic materials using SiO₂ nanofibres (SNF) and reduced graphene oxide (rGO) as the main raw materials, and the 2D layered structure of graphene oxide (GO) was used to fully entangle the SNF skeleton and block the pores of the fibre cavity wall. The two-dimensional layered structure of graphene oxide (GO) was used to fully entangle the SNF skeleton and block the pores of the fibre cavity wall to achieve multiple consumptions of acoustic waves, and the experimental results showed that the maximum sound absorption coefficient was 0.56. Zhang [37] used graphene oxide and polyurethane foam as raw materials to prepare lightweight, high-toughness porous acoustic materials, and the experimental results showed that the maximum acoustic absorption coefficient was 0.76.

Cellulose (CEL) aerogel has a porous structure, and its micropores and macropores are interconnected, which is conducive to improving sound absorption performance in the low-frequency range. Compared with other sound-absorbing materials such as graphene oxide, CEL-GO composite aerogels have high porosity, large specific surface area, low density, excellent mechanical properties, and chemical stability, and are an ideal porous sound-absorbing material [38]. In this paper, cellulose aerogels were prepared using lignocellulose and then composited with graphene oxide, taking full advantage of the lamellar structure of graphene oxide, which is tightly entangled with the cellulose skeleton, to create more semi-closed, closed, and long-range cavity structures for multiple depletion of acoustic waves. In this study, epichlorohydrin was also used as an auxiliary cross-linking agent. Epichlorohydrin can form a large number of hydrogen bonds with the hydroxyl group of the cellulose molecular chain due to its strong electronegative group, which is more helpful in improving the densification and cross-linking degree of the

composite aerogel material, which also improves the mechanical properties of the material. Therefore, we constructed acoustic absorbing materials with microscopic multi-walled cavity structures and complemented them with model validation, which provides a certain reference significance for subsequent studies.

2. Preparation and Characterisation of Materials

2.1. Materials Preparation of CEL-GO Composite Aerogels

A cellulose (fibre length > 20 μm , Shanghai Macklin Biochemical Technology Co., Ltd., Shanghai, China) dissolution system consisting of 7 wt.% NaOH:12 wt.% urea:81 wt.% H_2O was configured (NaOH and urea were analytically pure; Tianjin Fengchuan Chemical Reagent Co., Ltd., Tianjin, China). A total of 4 g of cellulose was added and mixed well, and then frozen at $-25\text{ }^\circ\text{C}$ for 20 h. The mixture was thawed at room temperature and frozen again, repeating the cycle 3 times. A transparent cellulose solution was obtained and 1/10 of its volume of epichlorohydrin (EC, analytically pure, Shanghai Macklin Biochemical Technology Co., Ltd.) was added as a cross-linking agent. It was shaken well at room temperature and allowed to solidify. Then, the excess cross-linking agent was washed with an aqueous ethanol solution (ethanol–distilled water ratio 1:10) until the gel was homogeneously dissolved, and the aerogel was obtained by lyophilisation for 48 h. This was recorded as CEL-EC for backup. In the next step, we first added 1 g of GO (multilayer, Suzhou Tanfeng Technology Co., Ltd., Suzhou, China) to 100 mL of distilled water, stirred thoroughly, and set the volume ratio gradient of the CEL solution and GO-water mixture to 0.5:1, 1:1, 2:1, and 3:1, and then added epichlorohydrin cross-linking agent to the mixture. The CEL-EC aerogel preparation steps were repeated as described above to prepare CEL-GO composite aerogels, labelled as CG-1, CG-2, CG-3, and CG-4, respectively.

2.2. Performance Characterisation of CEL-GO Composite Aerogels

The characteristics of the CEL-GO aerogel and the effect of GO on the crystalline shape of cellulose were analysed using X-ray diffractometry (D8advance, Bruker Co., Karlsruhe, Germany) with $\text{Cu K}\alpha$ radiation. In order to analyse the type of bonding and the presence of functional groups in the samples, Fourier transform infrared spectroscopy (INVENIO S, Bruker Co., Germany) was used in the wavelength range from 4000 cm^{-1} to 500 cm^{-1} , equipped with a Raman spectral analyser (RENISHAW, OPTOSKY Co., Xiamen, China). The microporous structure characteristics of the aerogel were investigated by scanning electron microscopy (Phenom Pro, PDSI Co., Shanghai, China) and fully automated specific surface area and porosity (BELSROP mini II, Bayer, Co., Osaka, Japan) analysis. At the same time, the density and porosity were calculated according to the national standard GB/T 6343-1995 [39], and the calculation results are shown in Table 1. Finally, we tested the acoustic absorption coefficients of the CEL aerogel and CEL-GO composite aerogel samples using JTZB standing wave tubes (JTZB, Beijing Century Jiantong Technology Development Co., Ltd., Beijing, China). The standing wave tube test system was equipped with JTSOFT-ZB professional software, which simultaneously acquired and displayed sound pressure signals, automatically generated sound absorption coefficients, and drew sound absorption curves. Based on the above theoretical analysis, we established an acoustic absorption mechanism model for the aerogel.

Table 1. The mass, density, and porosity analysis of the samples.

Samples	Mass (g)	Densities (g/cm^3)	Porosity (%)
CEL-CH	2.22	0.078	94.4
CEL-GO = 0.5:1	1.366	0.082	87.7
CEL-GO = 1:1	1.21	0.085	89.4
CEL-GO = 2:1	1.84	0.090	87.2
CEL-GO = 3:1	1.05	0.095	85.5

3. Results

Figure 1 shows the XRD patterns of the samples CEL, GO, and CEL-GO. It can be seen that the CEL sample has a clear distinct diffraction peak at $2\theta = 22.6^\circ$ in the (002) lattice plane and two overlapping diffraction peaks at $14^\circ \sim 17.8^\circ$, corresponding to the lattice plane of the cellulose I-type crystal structure. The GO sample (001) lattice plane has a distinct characteristic peak at $2\theta = 10.8^\circ$. From the patterns, it is clear that only the characteristic peaks of the group material appeared, and no other impurity peaks were observed. Furthermore, the lattice plane of the CEL-GO composite aerogel (002) shows the (002) crystal plane of CEL at $2\theta = 22.6^\circ$, but the diffraction peaks of the GO (001) crystal plane and the overlapping diffraction peaks of CEL are almost obscure, indicating that CEL bonded with GO [40].

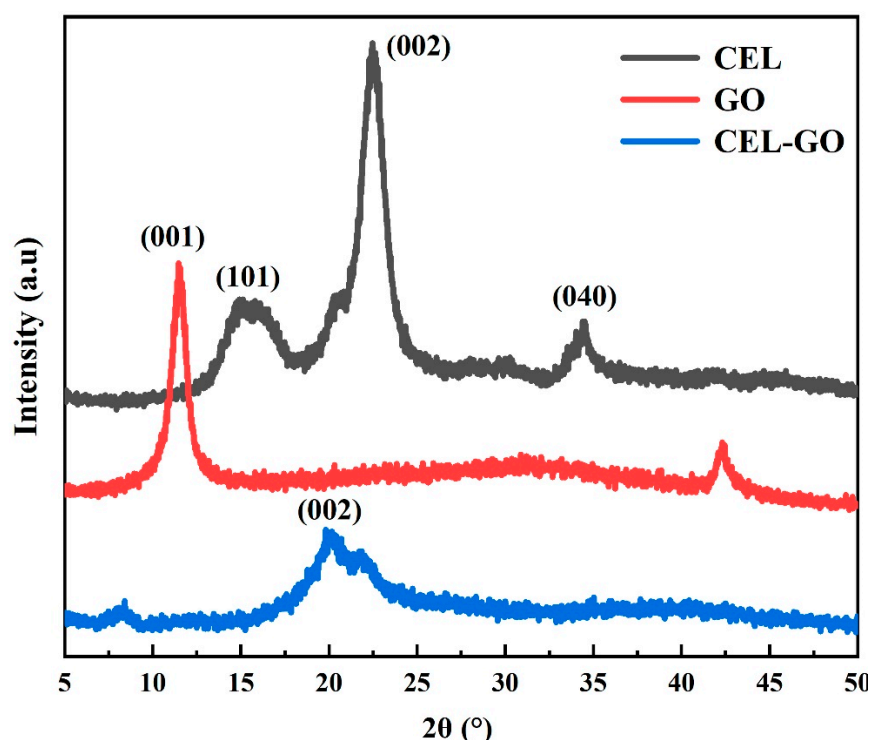


Figure 1. XRD patterns of CEL, GO, and CEL-GO.

To investigate the effect of GO addition on the structural composition of the CEL aerogel and the binding mode of GO and CEL, we performed Fourier infrared spectroscopy and Raman spectroscopy on the samples, and the results are shown in Figures 2 and 3. The stretching vibration peak of the hydroxyl group (3340 cm^{-1}) of CEL is clearly visible [41] in Figure 2, and the peaks corresponding to the stretching vibration peak of the methylene group of CEL are -CH_2 (2893 cm^{-1}) and C–C (895 cm^{-1}) [42]. The hydroxyl peak of CEL was attenuated when the ratio of CEL to GO was 0.5:1, which was attributed to the depletion of hydroxyl groups ($3200\text{--}3500\text{ cm}^{-1}$) by the reaction of GO with CEL and the use of the hydroxyl groups in CEL to form hydrogen bonds. In the CEL-GO composite aerogel material, there are backbone stretching vibration peaks of the benzene ring C=C (1430 cm^{-1}), absorption vibration peaks of C–O–C (1048 cm^{-1}), and stretching vibration peaks of C=O (1720 cm^{-1}), which represent GO [43], and a new ester group peak (1740 cm^{-1}) appeared in the CEL-GO composite aerogel material, indicating that GO successfully bonded to the CEL aerogel by forming a new chemical bond. In Figure 3, 2946 cm^{-1} is the C–H stretching vibration peak of CEL, and all CEL aerogels after GO composite have characteristic peaks representing graphene carbon materials, such as the G peak (1581 cm^{-1}) reflecting the characteristic peaks induced in the face of sp^2 carbon atoms, and the D peak (1350 cm^{-1}) indicating the characteristics of graphene such as defects and

vacancies [44]. The characteristic peaks that represent CEL are also found at 2946 cm^{-1} , which proves that the complexation of GO with CEL is successful.

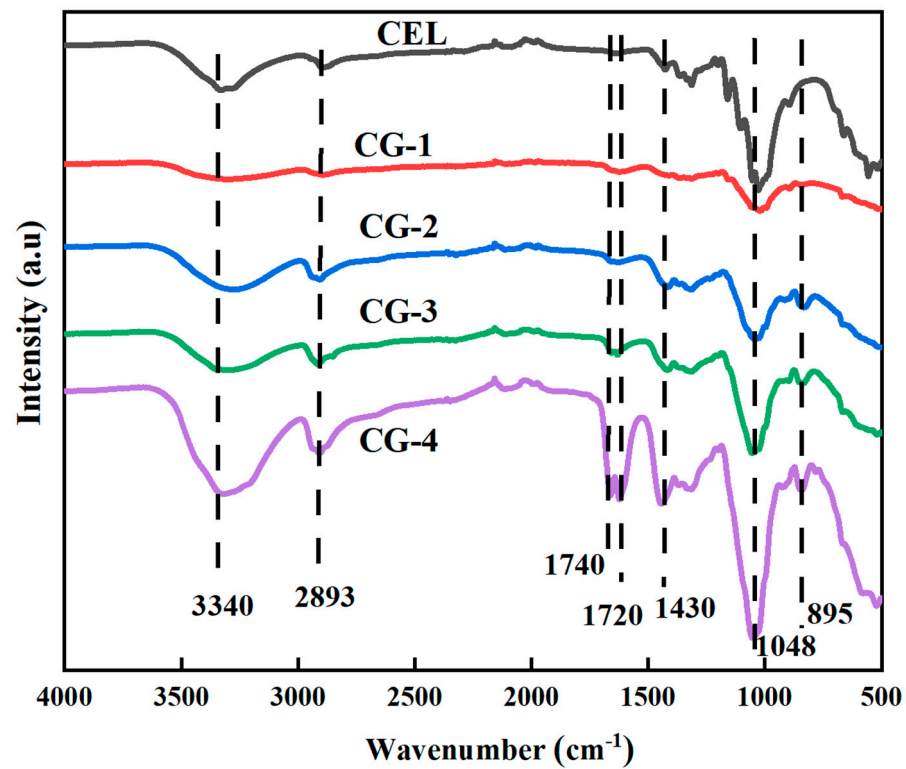


Figure 2. Infrared spectroscopy of CEL and CEL-GO composite aerogels.

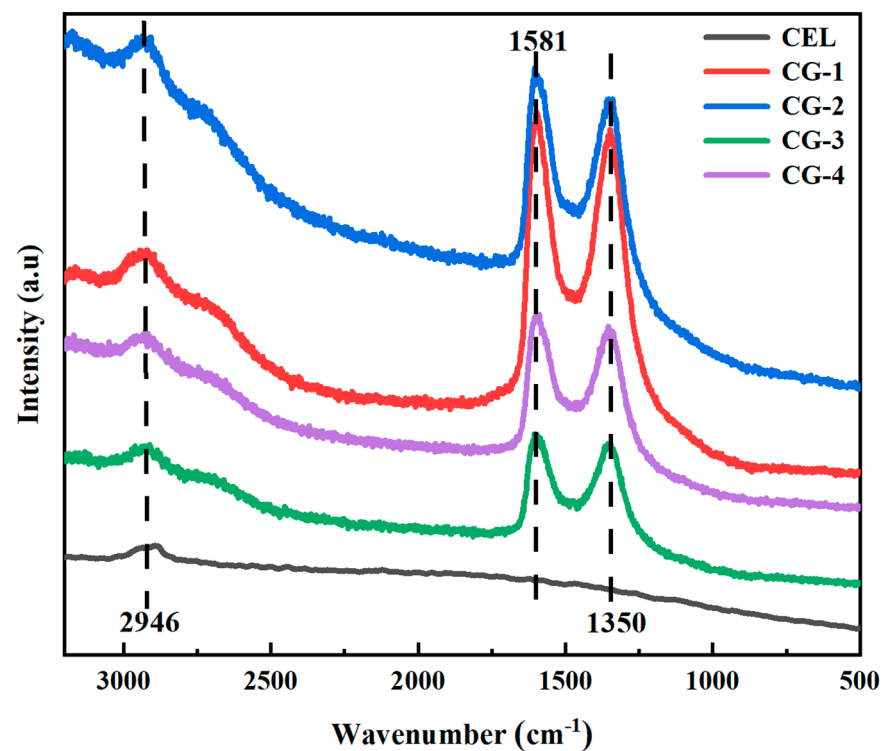


Figure 3. CEL-GO composite gas gel Raman spectroscopy analysis.

Figure 4 shows the SEM analysis of the CEL-GO composite aerogel. It can be seen that the addition of GO to the CEL solution formed a three-dimensional interconnected

pore structure with CEL molecules through hydrogen bonding and ionic bonding, which facilitated the dispersion of GO in the micropores of the aerogel and effectively improved the dispersion of GO in the CEL molecules [45]. With the increase in CEL content, the structure and performance of the CEL-GO composite aerogel were significantly improved. When the mass ratio was less than CEL:GO = 1:1, the flake GO was uniformly distributed on the framework of the CEL aerogel, the interface of GO and CEL was tightly crosslinked, and the flake GO played the role of enhanced toughening in the composite aerogel, which may be due to the combination of the functional groups of GO and the groups on the surface of CEL. The reason may be that the functional groups of GO combine with the groups on the surface of CEL to form hydrogen bonding, which prevents the agglomeration phenomenon of GO, increases the dislocation energy, and reduces the stress concentration [46]. In the marked area of Figure 4A, it can be clearly seen that graphene oxide is bonded to the cellulose skeleton in the form of lamellar layers and also forms a large number of polymorphic pore structures, such as long-range holes and multi-interface pore channel structures. When CEL:GO = 1:1, as shown in Figure 4B, especially in the marked area, a more homogeneous pore structure can be observed. This indicates that at this ratio, the combination of graphene and cellulose is denser and retains an appropriate pore structure, such as more closed or semi-closed pores and multi-boundary surface pores, which are beneficial for the material to absorb sound waves. However, if the CEL content is too high, it forms an amorphous structure, resulting in the loose structure of the CEL-GO composite aerogel, which cannot fully play the role of GO. As shown in Figure 4C,D, when the CEL:GO content exceeds 2:1, the interfibre spacing becomes smaller, resulting in a more compact macroporous structure of the porous aerogel, and the pore diameter tends to become smaller; this trend in the pore structure is equally evident in the marked areas of both figures, thereby reducing the acoustic absorption performance of the composite aerogel.

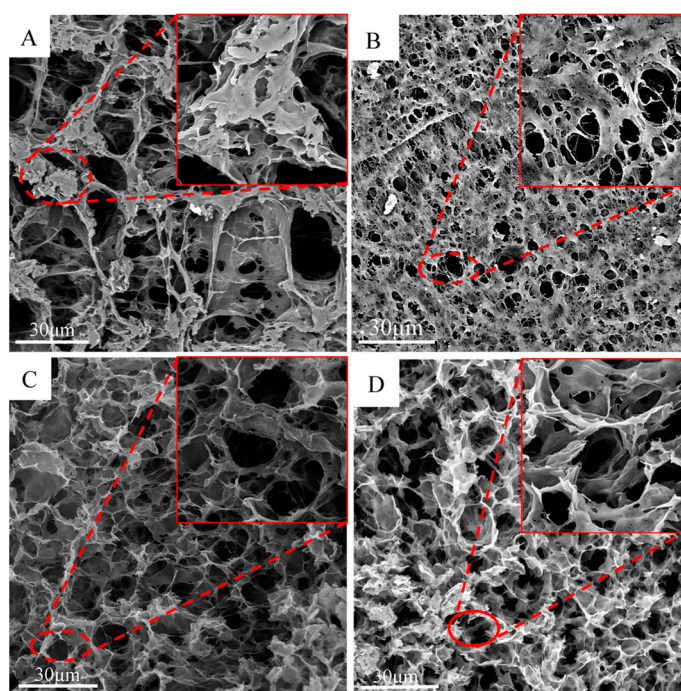


Figure 4. SEM analysis of CEL-GO composite aerogel. Pictures (A–D) correspond to aerogels in the ratios CEL:GO = 0.5:1; CEL:GO = 1:1; CEL:GO = 2:1; CEL:GO = 3:1.

The pore volume and pore size analyses of the CEL-GO composite aerogel are shown in Figure 5. The CEL aerogel shown in Figure 5a is a type II isotherm, demonstrating that it is dominated by large pores and that the pore structure is not uniformly distributed. As shown in Figure 5b, after the addition of GO to the CEL aerogel, the curve is a typical IV-type adsorption isotherm, and the nitrogen adsorption capacity of the CEL-GO com-

posite aerogel greatly improved compared with that of the pure CEL aerogels due to the improvement in the organisational structure of the composite aerogel by GO. The nitrogen adsorption capacity of the composite aerogel was the strongest when CEL:GO = 2:1, and the rising trend of the N₂ adsorption–desorption curves was slow when the relative pressure was 0.6 or less, which was caused by monomolecular layer adsorption. When the relative pressure is large, the N₂ adsorption–desorption curve rises rapidly and a hysteresis loop appears, which is due to a large number of mesoporous structures in the composite aerogel. The formation of hysteresis loops is due to the coalescence of capillary tubes, where the diameter of the curvature is shorter after coalescence, resulting in a lower pressure required for complete desorption, hence the formation of hysteresis loops [47].

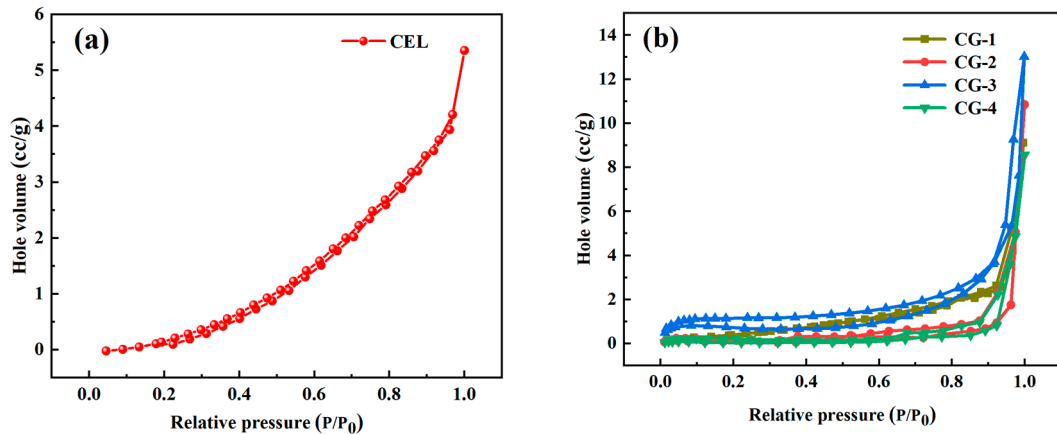


Figure 5. Aerogel nitrogen adsorption–desorption test: (a): CEL aerogel; (b): CEL-GO composite aerogel.

As shown in Figure 6a, the CEL aerogel has a high porosity and the pore size is mainly between 10 and 40 nm, indicating that the material has an internal mesoporous structure. As shown in Figure 6b, the pore size of the CEL-GO composite aerogel is mainly distributed between 0 and 20 nm, indicating that the presence of GO contributes to the formation of mesopores in the CEL aerogel. In addition, GO and CEL can also generate more hydrogen bonding interactions, which makes the molecules of CEL more tightly bound to each other, and this interaction not only promotes the formation of a more stable complex between the two but also helps to enhance the stability of GO in the function of the composite aerogel.

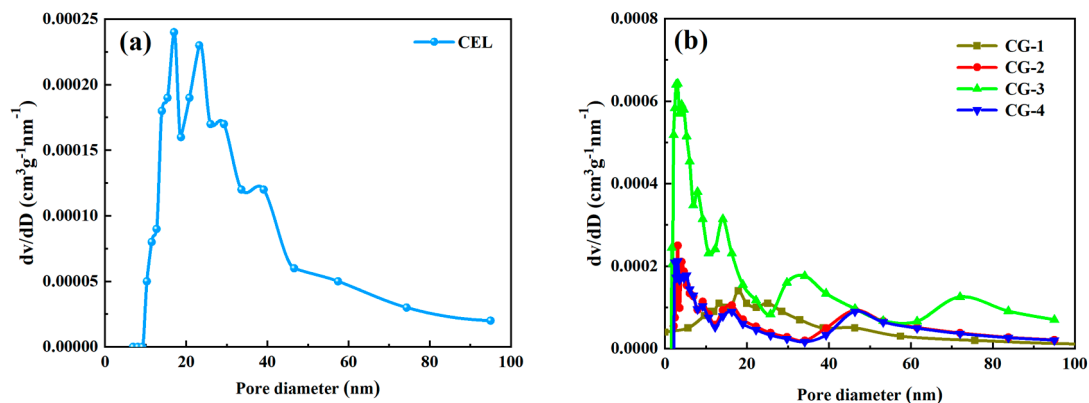


Figure 6. (a) CEL aerogel pore size distribution curve; (b) CEL-GO composite aerogel pore size distribution curve aerogel.

The density and porosity of the aerogel have a significant effect on the acoustic performance of the material. Aerogel contains a large number of internal pore structures, which is conducive to the penetration of acoustic waves, resulting in more pronounced

attenuation of the acoustic energy. The main reason why aerogel has a lower density is that it contains more pores inside and its pore ratio is greater than 85%. There are polar groups such as hydroxyl, ether, epoxy, and carboxylic acid. in GO, and GO has a high dispersing ability, which can be combined with CEL in the form of covalent bonds, ionic bonds, and hydrogen bonds, so it has good dispersing properties in the CEL aerogel, and since GO is a dense and porous carbon material, it can improve the acoustic performance of CEL-GO composite aerogels [48]. With an increase in the CEL content, the pores inside the aerogel are occupied by the increased solid CEL, resulting in a gradual decrease in porosity; thus, a negative correlation between the density and porosity change trend is obtained, and the acoustic performance of the composite aerogel is therefore decreased. And the composite aerogels with different GO additions, densities, and porosity analysis data are shown in Table 1.

As shown in Figure 7, the sound absorption coefficient of the CEL-GO composite aerogel is higher than that of the pure CEL aerogel, with a peak at 2000 Hz. The peak gradually moves toward the high-frequency direction, with an average absorption coefficient of more than 0.8, and the highest absorption coefficient of 0.87 is 2000 Hz–6000 Hz. The CEL molecular chains are connected to the CEL molecules via hydrogen bonding and van der Waals forces, and these two forces play a key role in the intertwining of the CEL molecules, contributing to their high diffusion performance in the whole network. Thus, they can greatly affect the pore size of the aerogel and the acoustic performance of the aerogel [48]. GO is a two-dimensional planar-structured nanomaterial with good dispersion properties; its layered porous structure is used to increase the acoustic wave transmission paths, and the acoustic wave is dissipated in the form of thermal energy, which is a new type of sound absorption and noise reduction material [49]. The introduction of GO into the CEL aerogel can improve the internal pore structure while maintaining the original excellent acoustic performance of the CEL aerogel, thus improving its acoustic performance. The introduction of GO provides a way to physically increase the capacity of the CEL aerogel so that the increase in internal pore space is conducive to the acoustic performance of the CEL aerogel.

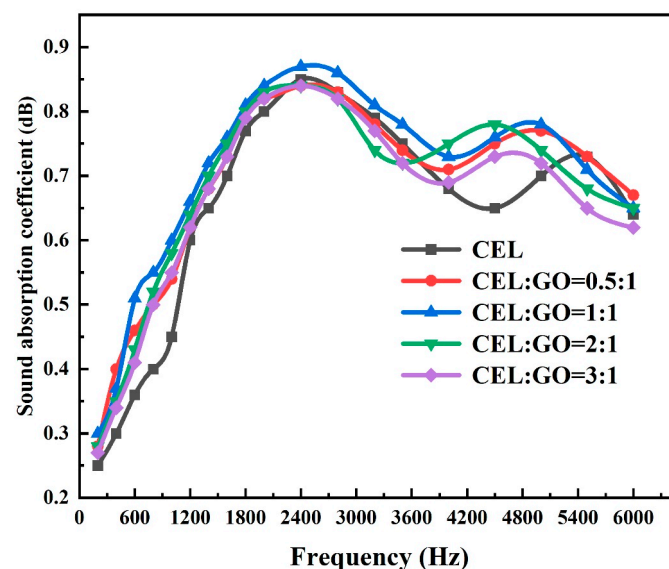


Figure 7. Sound absorption performance analysis of CEL-GO composite aerogel.

Based on the theoretical analysis of the above tests, we constructed a molecular structure model of the composite aerogel as shown in Figure 8. From Figure 8, it can be seen that the CEL chain contains abundant hydroxyl (-OH) and carboxyl (-COOH) groups, and PVA contains a large number of oxygen-containing functional groups, such as hydroxyl (-OH), carboxyl (-COOH), carbonyl (-C=O), and epoxy (-CH₂O) [50]. The molecular chain of CEL interacts with the molecules of PVA via both chemical bonding and hydrogen

bonding, and thus the PVA-modified CEL aerogel is rich in pore structure and has a thicker pore wall, which shows good mechanical properties and acoustic properties. The acoustic performance of the CEL aerogel is closely related to the size and distribution of its internal pores, and GO changes the intermolecular interactions of CEL to a certain extent, which improves the overall performance of the CEL aerogel [51]. The GO-modified CEL aerogel showed excellent acoustic performance, and after freeze-drying, the morphology of the CEL aerogel was a three-dimensional network structure. GO and PVA played a scaffolding role between the fibres, and the specific surface area of the CEL aerogel was effectively improved, which was conducive to increasing its internal pores [52].

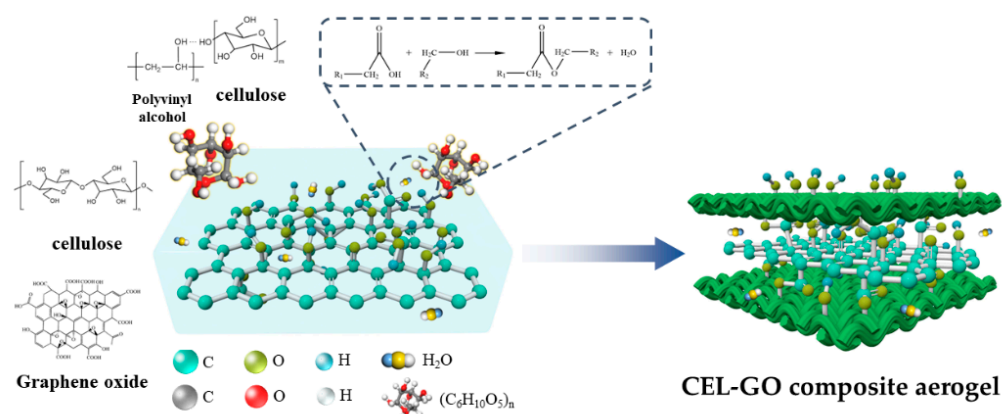


Figure 8. The molecular structure model of sound absorption mechanism of CEL-GO composite aerogel.

4. Conclusions

Using various characterisation tests and theoretical analyses of the samples, we successfully prepared CEL-GO aerogel materials with high acoustic absorption performance, and the highest acoustic absorption coefficient was up to 0.87. We also verified the bonding modes of the two-component materials, based on which we constructed a molecular structure model of the acoustic absorption mechanism of the composite materials. The specific conclusions are as follows: (1) The new peak at 1740 cm^{-1} in the infrared spectrum indicates that an esterification reaction occurred between GO and CEL, and a new chemical bond was formed in the CEL-GO composite aerogel material. (2) From the nitrogen adsorption–desorption test, it can be seen that the nitrogen adsorption capacity of the CEL-GO composite aerogel greatly improved compared with that of the pure CEL aerogel, and the number and size of the microstructure of the composite aerogel were improved and optimised by GO; it was found that the CEL-GO composite aerogel had characteristic peaks of G (1581 cm^{-1}) and D (1350 cm^{-1}) and a characteristic peak of CEL (2946 cm^{-1}), which proved that GO and CEL were successfully composited. (3) With an increase in the CEL content, the internal porosity of the aerogel decreased and the density increased, and the density and porosity showed a negative correlation trend; the CEL aerogels composited by GO had a higher acoustic absorption coefficient than that of the pure CEL aerogel, and the highest acoustic absorption coefficient reached 0.87.

Author Contributions: J.S.: designed the study, performed experiments, analysed the data, and wrote the manuscript. Y.L.: performed the experiments and analysed the data. Z.X.: conceptualisation, methodology, resources, and manuscript revision. Y.P.: conceptualisation and methodology. J.L.: methodology and experimentation. M.D.: manuscript revision. F.Q.: methodology. All authors have read and agreed to the published version of the manuscript.

Funding: This work was supported by the National Natural Science Foundation of China (31860187).

Institutional Review Board Statement: Not applicable.

Informed Consent Statement: Not applicable.

Data Availability Statement: The data used to support the findings of this study are available from the corresponding author upon request.

Acknowledgments: We are grateful to the National Natural Science Foundation of China (31860187) for the financial support of this work, to the School of Material Science and Art Design of Inner Mongolia Agricultural University for providing the physical and chemical experimental platform for the work, to the Key Laboratory of Fibrillation and Energy Recovery and Utilisation of Salix Resources of Inner Mongolia Autonomous Region for providing all kinds of experimental raw materials and relevant testing instruments for the work, to the authors of the work for their full cooperation, and to the supervisors for their detailed guidance.

Conflicts of Interest: The authors declare no conflicts of interest.

References

1. Zhao, H.; Jiang, N. Research on Substation Noise and Design of the Control System. *J. Mod. Power Syst. Clean Energy* **2015**, *31*, 55–60.
2. Sun, P. *Preparation of Porous Sound-Absorbing Material Using Steel Slag and Its Sound Absorption Properties*; University of Science and Technology Beijing: Beijing, China, 2016.
3. Liu, K. Simulation Research on the Application of Porous Sound-absorbing Material Based on VA One. *Transp. Sci. Technol.* **2010**, *2*, 4.
4. Cao, L. Porous materials for sound absorption. *Compos. Commun.* **2018**, *10*, 25–35. [[CrossRef](#)]
5. Schiavoni, S. Insulation materials for the building sector: A review and comparative analysis. *Renew. Sustain. Energy Rev.* **2016**, *62*, 988–1011. [[CrossRef](#)]
6. Forouharmajd, F. Assessment of normal incidence absorption performance of sound absorbing materials. *Int. J. Environ. Health Eng.* **2016**, *5*, 10.
7. Yang, T. Sound absorption properties of natural fibers: A review. *Sustainability* **2020**, *12*, 8477. [[CrossRef](#)]
8. Asdrubali, F. A review of unconventional sustainable building insulation materials. *Sustain. Mater. Technol.* **2015**, *4*, 1–17. [[CrossRef](#)]
9. Liu, L. The development history and prospects of biomass-based insulation materials for buildings. *Renew. Sustain. Energy Rev.* **2017**, *69*, 912–932. [[CrossRef](#)]
10. Hill, C. A comparison of the environmental impacts of different categories of insulation materials. *Energy Build.* **2018**, *162*, 12–20. [[CrossRef](#)]
11. Papadopoulos, A.M. Environmental performance evaluation of thermal insulation materials and its impact on the building. *Build. Environ.* **2007**, *42*, 2178–2187. [[CrossRef](#)]
12. Xia, Q. A strong, biodegradable and recyclable lignocellulosic bioplastic. *Nat. Sustain.* **2021**, *4*, 627–635. [[CrossRef](#)]
13. Iñaki, G. Biomimetic Wood-Inspired Batteries: Fabrication, Electrochemical Performance, and Sustainability within a Circular Perspective. *Adv. Sustain. Syst.* **2021**, *5*, 2100236.
14. CRIWI. *The Physical and Mechanical Properties of the Main Tree Species in China*; China Forestry Press: Beijing, China, 1982.
15. Li, J. *Wood Science*, 3rd ed.; Science Press: Beijing, China, 2014.
16. Zhao, G.J. Nanoscale, Nanowood, and Wood Inorganic Nanocomposites in Wood. *J. Beijing For. Univ.* **2002**, *24*, 204–207.
17. Xue, Z.H. Theoretical Evaluation of Wood Voids. *J. Inn. Mong. Agric. Univ.* **2009**, *30*, 252–257.
18. Lin, M.D. Estimating the sound absorption coefficients of perforated wooden panels by using artificial neural networks. *Appl. Acoust.* **2009**, *70*, 31–40. [[CrossRef](#)]
19. Asdrubali, F. A review of structural, thermo-physical, acoustical, and environmental properties of wooden materials for building applications. *Build. Environ.* **2017**, *114*, 307–332. [[CrossRef](#)]
20. Kang, C. Changes in anatomical features, air permeability and sound absorption capability of wood induced by delignification treatment. *Kyushu Univ.* **2008**, *53*, 479–483. [[CrossRef](#)] [[PubMed](#)]
21. Kolya, H. High acoustic absorption properties of hackberry compared to nine different hardwood species: A novel finding for acoustical engineers. *Appl. Acoust.* **2020**, *169*, 107475. [[CrossRef](#)]
22. Chen, C. Structure–property–function relationships of natural and engineered wood. *Nat. Rev. Mater.* **2020**, *5*, 642–666. [[CrossRef](#)]
23. Li, J. In situ wood delignification toward sustainable applications. *Acc. Mater. Res.* **2021**, *2*, 606–620. [[CrossRef](#)]
24. Guan, H. Highly compressible wood sponges with a spring-like lamellar structure as effective and reusable oil absorbents. *ACS Nano* **2018**, *12*, 10365–10373. [[CrossRef](#)]
25. Song, J. Highly compressible, anisotropic aerogel with aligned cellulose nanofibers. *ACS Nano* **2018**, *12*, 140–147. [[CrossRef](#)]
26. Li, T. Anisotropic, lightweight, strong, and super thermally insulating nanowood with naturally aligned nanocellulose. *Sci. Adv.* **2018**, *4*, 3724. [[CrossRef](#)]
27. Zhu, M. Highly anisotropic, highly transparent wood composites. *Adv. Mater.* **2016**, *28*, 5181–5187. [[CrossRef](#)]
28. Wang, J. Carbonate pre-treatment of wood for transformative structural applications through densification. *Ind. Crops Prod.* **2022**, *183*, 188. [[CrossRef](#)]
29. Sun, J. Enhanced mechanical energy conversion with selectively decayed wood. *Sci. Adv.* **2021**, *7*, eabd9138. [[CrossRef](#)]

30. Zhao, X. A scalable high-porosity wood for sound absorption and thermal insulation. *Nat. Sustain.* **2023**, *6*, 306–315. [[CrossRef](#)]
31. Kolya, H. Ammonium persulfate treatment on carbohydrate polymers and lignin of wood improved sound absorption capacity. *Int. J. Biol. Macromol.* **2022**, *205*, 626–637. [[CrossRef](#)]
32. Zhu, X.D. The current research status of sound absorption performance of wood plastic composite materials. *J. For. Eng.* **2017**, *2*, 10–15.
33. Zhou, D.D.; Fang, L.; Yang, Q.Z. Preparation and performance of base magnesium sulfate porous sound absorbing materials. *CIESC J.* **2021**, *72*, 3041–3052.
34. Lize, Q.; Chao, Z.J. Highly efficient acoustic absorber designed by backing cavity-like and filled-microperforated plate-like structure. *Mater. Des.* **2023**, *225*, 111484.
35. Pang, K.; Liu, X.; Pang, J.; Samy, A.; Xie, J.; Liu, Y.; Peng, L.; Xu, Z. Highly Efficient Cellular Acoustic Absorber of Graphene Ultrathin Drums. *Adv. Mater.* **2022**, *34*, 2103740. [[CrossRef](#)]
36. Zong, D.; Cao, L.; Yin, X.; Si, Y.; Zhang, S.; Yu, J.; Ding, B. Flexible ceramic nanofibrous sponges with hierarchically entangled graphene networks enable noise absorption. *Nat. Commun.* **2021**, *12*, 6599. [[CrossRef](#)]
37. Zhang, H.; Wang, H.; Wang, T.; Han, S.; Zhang, X.; Wang, J.; Sun, G. Polyurethane Foam with High-Efficiency Flame Retardant, Heat Insulation, and Sound Absorption Modified by Phosphorus-Containing Graphene Oxide. *ACS Appl. Polym. Mater.* **2024**, *6*, 1878–1890. [[CrossRef](#)]
38. He, S.H. Development status and prospect of cellulose based foam and aerogel porous materials. In *Collected Papers from the 19th Academic Annual Conference of the Chinese Paper Society*; Chinese Paper Society: Beijing, China, 2020; pp. 451–463.
39. ISO 845:2006; Cellular Plastics and Rubbers-Determination of Apparent Density. ISO: Geneva, Switzerland, 2006.
40. Liu, T. Highly compressible anisotropic graphene aerogels fabricated by directional freezing for efficient absorption of organic liquids. *Carbon* **2016**, *100*, 456–464. [[CrossRef](#)]
41. Vázquez, G. FTIR, ¹H and ¹³C NMR Characterization of Acetosolv-Solubilized Pine and Eucalyptus Lignins. *Holzforschung* **1997**, *51*, 158–166. [[CrossRef](#)]
42. Lin, Y. Preparation and characterisation of covalent polymer functionalized graphene oxide. *J. Mater. Chem.* **2011**, *21*, 3455–3461. [[CrossRef](#)]
43. Jiang, S.T. Preparation and Absorption Property of GO/Nanocellulose Composite Aerogel. *New Chem. Mater.* **2020**, *48*, 81–84+89.
44. Silviana, S. Optimizing the environmentally friendly silica-cellulose aerogel composite for acoustic insulation material derived from newspaper and geothermal solid waste using a central composite design. *J. Sol-Gel Sci. Technol.* **2022**, *103*, 226–243. [[CrossRef](#)]
45. Lin, D.H. Preparation and Properties of NFC Composite Aerogel Supercapacitors. *Pap. Sci. Technol.* **2017**, *36*, 28–35.
46. Liu, X. Fabrication of hydrogel of hydroxypropyl cellulose (HPC) composited with graphene oxide and its application for methylene blue removal. *J. Mater. Sci.* **2015**, *50*, 6113–6123. [[CrossRef](#)]
47. Klem, D. Nanocelluloses: A new family of nature-based materials. *Angew. Chem. Int. Ed.* **2011**, *50*, 5438–5466. [[CrossRef](#)]
48. Rapisarda, M. Multifunctional Thermal, Acoustic, and Piezoresistive Properties of In Situ-Modified Composite Aerogels with Graphene Oxide as the Main Phase. *ACS Appl. Mater. Interfaces* **2022**, *14*, 43646–43655. [[CrossRef](#)]
49. Tao, Y. Recent progress in acoustic materials and noise control strategies—A review. *Appl. Mater. Today* **2021**, *24*, 101141. [[CrossRef](#)]
50. Wang, J.Q. Research progress and prospects of performance of kinetic hydrate inhibitor and effect of functional group. *J. Cent. South Univ.* **2022**, *53*, 772–798.
51. Yao, Q. 3D assembly based on 2D structure of cellulose nanofibril/graphene oxide hybrid aerogel for adsorptive removal of antibiotics in water. *Sci. Rep.* **2017**, *7*, 45914. [[CrossRef](#)]
52. Rapisarda, M. Ultralight graphene oxide/polyvinyl alcohol aerogel for broadband and tuneable acoustic properties. *Sci. Rep.* **2021**, *11*, 10572. [[CrossRef](#)]

Disclaimer/Publisher’s Note: The statements, opinions and data contained in all publications are solely those of the individual author(s) and contributor(s) and not of MDPI and/or the editor(s). MDPI and/or the editor(s) disclaim responsibility for any injury to people or property resulting from any ideas, methods, instructions or products referred to in the content.